Inorganic Chemistry

Article

pubs.acs.org/IC

Ammonium Tetrathiomolybdate: A Versatile Catalyst for Hydrogen Evolution Reaction from Water under Ambient and Hostile Conditions

Sudipta Chatterjee, Kushal Sengupta, Subal Dey, and Abhishek Dey*

Department of Inorganic Chemistry, Indian Association for the Cultivation of Science, Kolkata, India, 700032

Supporting Information

ABSTRACT: The lack of catalysts that can selectively reduce protons to produce hydrogen from water in the presence of oxygen and other conventional inhibitors of hydrogen evolution reaction (HER) has been a fundamental problem stalling the development of a practical hydrogen economy. Ammonium tetrathiomolybdate (ATM), a common laboratory reagent, spontaneously assembles on Au electrodes. Atomic force microscopy, scanning electron microscopy, and X-ray photoelectron spectroscopy data indicate formation of multiple layers of ATM which are stable over a wide pH range for days. These assemblies can produce hydrogen with very low onset potentials. It shows a turnover rate of 1.4 s^{-1} and turnover number $>5 \times 10^4$ in pH 7 at 180 mV overpotential. The pH dependence of the peak potential suggests that the generation of H_2 from water proceeds likely via a ligand based proton coupled electron transfer process which precludes inhibition by O_2. The ATM functionalized Au electrodes are found to efficiently catalyze HER in saline rich, CO saturated, and sulfide rich water sources with minimal inhibition of catalytic activity.

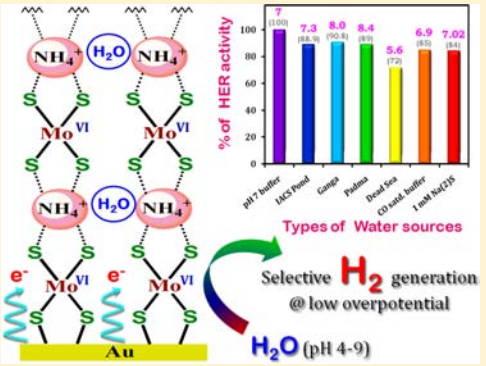

INTRODUCTION

A H_2 based fuel economy is hailed as a probable alternative to the conventional fossil fuel based economy.[1,2] The advantages of using H_2 as an energy vector have been widely discussed and need no further introduction.[3,4] However a practical wide-scale implementation of such a scheme is currently limited by the stringent availability of cheap and efficient catalysts for hydrogen evolution reaction (HER).[5] A cheap catalyst, by definition, requires easy availability and affordable synthesis. An efficient catalyst must have reasonable rates at low overpotentials, significant durability, selectivity toward H^+ reduction and retention of activity in water obtained from locally available sources.[6,7] In this regard, efforts over the past few years have seen several catalysts that possess a combination of these properties but not all of them (Table 1). Several molybdenum,[8−16] cobalt,[5,17−21] iron,[22,23] and nickel[24,25] based catalysts are reported to evolve H_2 from water at different pHs, and some of them show reasonable rates and stabilities in deoxygenated environments. While some of them have shown limited stability under oxic conditions,[26,27] it is important to retain optimal activity and, as a best case scenario, be selective toward reducing H^+ over O_2, which is a much stronger oxidant relative to H^+ present in untreated water. Almost all HER catalysts use a low-valent metal center with an open coordination site for H^+ binding. H^+, the oxidant, binds at this site and gets reduced to H_2. Logically this system, honed for inner-sphere reduction of small molecules, falls prey to O_2 easily because of its higher oxidation potential as well as solubility in water. This limitation is not unique to these artificial catalysts, as hydrogenases (H_2ase), the naturally occurring enzyme responsible for H_2 production from water shares the same weakness.[28−30] There are two ways to deal with this problem. One way is to reduce O_2 as well as H^+ using the catalyst as is the case for noble metal based electrodes. While this may give the catalyst a larger lifetime (provided it catalyzes $4e^-/4H^+$ reduction of O_2 to H_2O as partial reduction of O_2 to O_2^- or H_2O_2 leads to catalyst degradation), this reduces the efficiency of the process, as much of the reducing equivalent (in the form of cathodic current or photochemically generated electrons) is lost in reducing O_2.[26] The other, and the most efficient option, is to reduce H^+ selectively in the presence of O_2. This is a daunting task if only a metal based H^+ reduction pathway is considered.[31,32] Hence none of the HER catalysts reported this far, except that reported by Reisner's group,[26] clearly demonstrate any selectivity for HER over the competing oxygen reduction reaction (ORR). In several proposed mechanisms, a protonated ligand acts as a proton source to a metal hydride facilitating the formation of H_2.[12,33−36] Apart from such ligand assisted mechanisms, there has been discussion on a possible ligand based mechanism.[33] Here the metal center does not need to bind a proton to reduce it to a hydride and hence may provide a mechanism of avoiding ORR by the metal as well. Thus far no system has experimentally demonstrated this selectivity.

Received: August 9, 2013
Published: November 21, 2013

   dx.doi.org/10.1021/ic402056k | Inorg. Chem. 2013, 52, 14168−14177

Table 1. Kinetic Properties of Complexes and Materials That Catalyze HER in Water

catalyst	pH	onset potential (vs RHE)	Faradaic yield (FY in %)		catalytic parameters		
			N_2	O_2	TOF (s^{-1})	TON	η_{cat}[a] (mV)
[16] MoS_3	0	−0.12 V	∼100		2		240
[27] Co−F_8	0.3	−0.28 V		52	600	$>10^7$	680
[23] BrC_6H_4-$(CH_2S)_2$ Fe_2 $(CO)_6$	0.3	−0.28 V	>95		6000	$>10^8$	480
[8,47] MoS_2	0.3	−0.18 V			0.3		200
[48] Co-tetraaza macrocycles	2.2	−0.27 V	81			23	550
[10] $[(PY5Me_2)MoS_2]^{+2}$	3.0	−0.47 V	∼100		280	3.5×10^3	828
[21]GDL/MWCNT/Co	4.5	−0.35 V	97		2.2	5.5×10^4	590
[49] $[Mo_{12}DFMT]^{2-}$	6.0	−0.29 V	82			23	320
$(NH_4)_2[MoS_4]$	4.0−9.0	∼ −0.02 V	92	89	1.4	$>5 \times 10^4$	180
[26] $[CoP]^-$	7.0	−0.14 V	68	43	0.02		280
[9] $[(PY5Me_2)MoO]^{+2}$	7.0	−0.52 V			2.4	6.1×10^5	980
[20] H_2−CoCat	7.0	−0.05 V	∼100		0.02		385
[12] Cu_2MoS_4	7.0	−0.13 V	∼100			1.1×10^3	400
[18] Co-pentapyridine	7.0	−0.66 V	∼100		0.3	5.5×10^4	880

[a] η_{cat} represents the overpotential at which the TON and TOF are evaluated vs RHE.

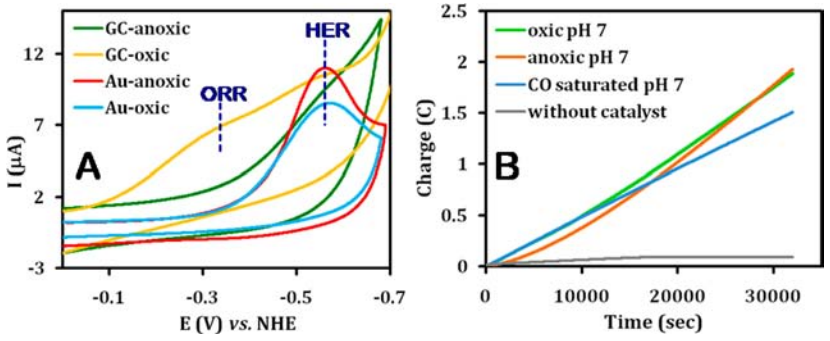

Figure 1. (**A**) CV data of 1 mM ATM solution in pH 7 buffer using GC and Au as working electrodes under both oxic conditions (yellow and blue, respectively) and anoxic conditions (green and red, respectively), using Ag/AgCl as reference (data have been adjusted to potential vs NHE) and Pt wire as counter electrodes. (**B**) Plot of the charge consumed vs time elapsed during controlled potential electrolysis (CPE) experiments of 1 mM ATM solution in pH 7 using Au as working electrode under oxic (green), anoxic (red) and CO saturated (blue) conditions using Ag/AgCl as reference and Pt wire as the counter electrodes. The data obtained by bare Au in the absence of catalyst is shown in gray. Note that the working electrode during electrolysis experiment was held at the peak potential (−0.55 V vs NHE) obtained from CV.

Recently, several studies have reported HER by neutral MoS_x and WS_x material under acidic conditions.[16,37−39] Among them, reports by Hu's group on HER activity by amorphous MoS_x seems most efficient, showing an onset potential of about 150−200 mV vs RHE.[16,40] They extensively studied the growth and activation of these materials on Au and glassy carbon substrates and reported current densities as high as 20 mA/cm^2 at an overpotential of 170 mV with 200 μg/cm^2 loading.[41] Theoretical and experimental studies done by Chorkendorff's and Jaramillo's group show that the edges of the triangular MoS_2 nanocrystals are the likely active sites for HER.[8,33,42] Dai's and Liu's group demonstrated in their works that MoS_2 grafted graphene surfaces show effective electrocatalytic HER at even lower overpotentials.[43,44] Similar observations have been reported by Huang's group which established that MoS_2/Au and WS_2/Au hybrids were more effective toward HER activity than their undecorated counterparts.[39] Recently, Li's group showed enhanced electrocatalytic HER activity from self-assembled monodispersed MoS_2 nanoparticles on Au electrodes with an onset potential of about 90 mV.[45] Ammonium tetrathiomolybdate (ATM) is a cheap laboratory reagent which is used for many common organic transformations and serves as the precursor to all the neutral MoS_x materials and Cu_2MoS_4, known to produce H_2 from acidic H_2O.[8,11,12,43,46] However, HER activity of ATM itself is still unexplored.

In this report we show that ATM can reduce H_2O to produce H_2 in the presence of O_2. ATM selectively catalyzes HER in oxic environment (i.e., no ORR) when an Au surface is used as the electrode. This is due to formation of ordered assembly of ATM on Au surfaces. These ATM assemblies are stable and produce H_2 from water over a wide range of pH near its thermodynamic potential. The low overpotential of the catalyst results in exchange current densities orders of magnitude higher than any reported electrocatalyst and comparable to those observed for noble metals. The catalytic process involves a ligand based mechanism, and not a metal based mechanism which makes this catalyst effective even in the presence of toxins like CO,[31,36] S^{2-}/HS^-, and so forth which inhibit HER catalysis by noble metal electrodes, molecular complexes, as well as the natural enzyme. The ligand based mechanism allows uninhibited HER in water obtained from natural water bodies including the Dead Sea.

RESULTS AND DISCUSSION

Cyclic voltammetry (CV) of ATM using a glassy carbon electrode (GC) shows two electrocatalytic processes, one at

dx.doi.org/10.1021/ic402056k | Inorg. Chem. 2013, 52, 14168−14177

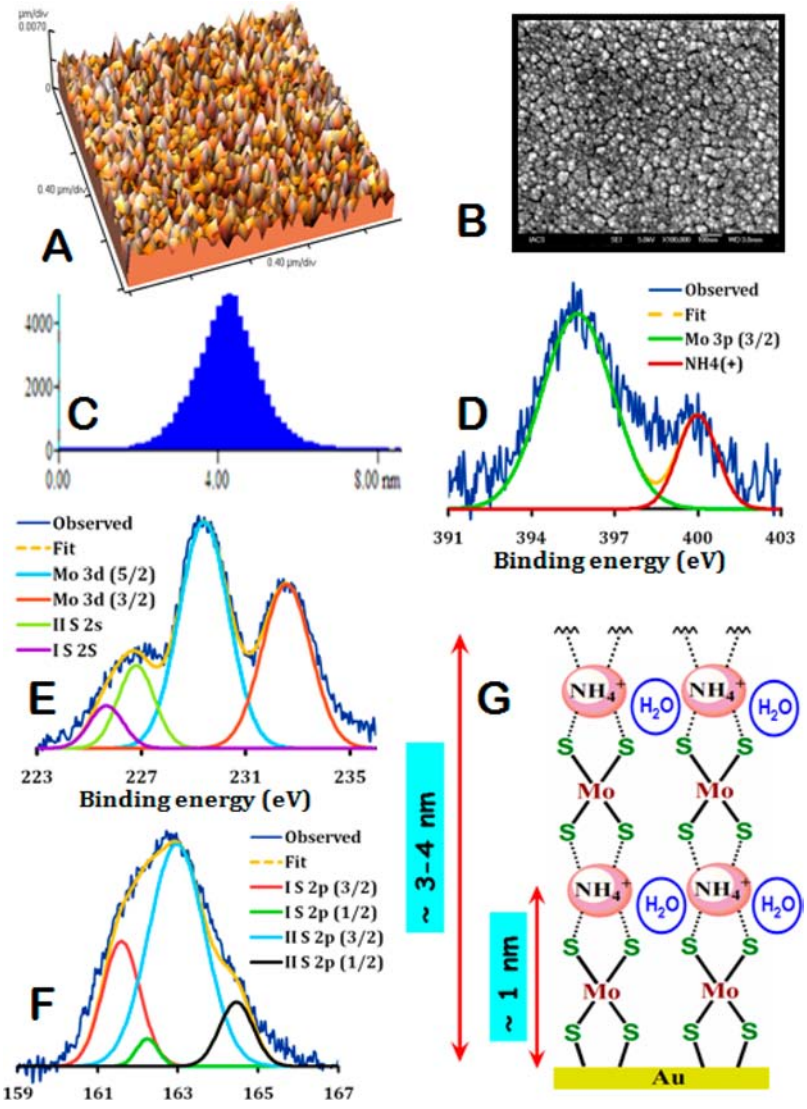

Figure 2. (**A**) AFM data of ATM modified Au electrodes; (**B**) FE-SEM image of a similar modified surface prepared from a 1 mM ATM solution; (**C**) Height distribution profile of the self-assembled layers of ATM on Au electrode observed by AFM experiment; (**D**), (**E**), and (**F**) XPS data of ATM modified Au electrode showing different regions along with their best fits showing the various components. (**G**) Vertical cross section of a probable three-dimensional ATM assembly on an Au electrode where the MoS_4^{2-} anions are held by the NH_4^+ ions by electrostatic and hydrogen bonding interactions.

−0.3 V and the other at −0.55 V, under oxic conditions and only the lower potential process at −0.55 V under anoxic conditions (Figure 1A). The process at −0.3 V is present even in the absence of ATM in solution in aerated buffers and represents O_2 reduction by a bare GC electrode. In the presence of ATM in solution in addition to this O_2 reduction process a lower potential process is present at −0.55 V (Figure 1A) and represents electrocatalytic H_2 evolution by ATM (vide infra). However, when an Au working electrode is used (an Au wire, an Au disc, an Au wafer or a standard 0.2 cm diameter polished Au electrode), only the lower potential process is observed both under oxic and anoxic conditions (Figure 1A). Since electrochemical ORR can not proceed under anoxic conditions, the process observed under both anoxic and oxic conditions must reflect HER, that is, when an Au working electrode is used ATM catalyzes HER selectively even in the presence of O_2.

Bulk electrolysis (BE) experiments conducted in a 1 mM ATM solution at pH 7 using GCE show a much higher current under oxic conditions relative to the current obtained under anoxic conditions (Supporting Information, Figure S1). This is because under oxic conditions, both O_2 ($4H^+/4e^-$) and H^+ ($1H^+/1e^-$) are reduced whereas under anoxic conditions only H^+ is reduced. However, when an Au electrode is used, there is no difference in the electrolysis current observed under oxic or anoxic environments (Figure 1B). This suggests that the selective HER reactivity of ATM in the presence of O_2 is retained even during long-term electrolysis. Over a period of 10 h, using a 0.1925 cm^2 Au electrode, 4.26 C charge was delivered and 0.44 ± 0.02 mL of H_2 was evolved from a 1 mM solution of ATM under oxic condition (Supporting Information, Figure S2). Similar experiment under anoxic condition yielded 0.46 ± 0.01 mL of H_2 while a charge of 4.32 C of charge was delivered (Supporting Information, Figure S2). These results indicate that the catalyst has a Faradaic yield (FY) of 89 ± 2% under oxic conditions and 92 ± 1% under anoxic conditions for HER. Note that the HER rate is slightly lower (showing a delayed onset) under anoxic conditions relative to oxic conditions

dx.doi.org/10.1021/ic402056k | Inorg. Chem. 2013, 52, 14168−14177

during BE experiments. This trend holds even when the BE experiments are performed at different potentials (Supporting Information, Figure S3) and may indicate some minor ORR activity in the CPE time scale. The marginally lower FY observed under oxic conditions may be due to this minor ORR activity.

Hu et al. has recently shown that the HER activity is unabated for amorphous MoS_3 on a rotating carbon disc electrode even in presence of CO.[37] DuBois et al. has reported a molybdenum−sulfur dimer ($Cp_2Mo_2S_4$) which is also insensitive toward CO retaining 80% of its catalytic activity.[36] The HER catalyzed by ATM on Au proceeds normally, showing about 85% activity, when the aqueous solution is saturated with CO (vide infra), a common inhibitor of most noble metal based HER catalysts. The reduction in HER activity in all the above cases is due to reaction with CO as proposed by DuBois.

Bare Au electrodes are known to catalyze ORR[50−52] in pH 7 buffer solutions. However, when immersed in aqueous ATM solutions for more than 20 min, they do not exhibit ORR (Supporting Information, Figure S4). Instead they exhibit only HER activity in aqueous buffer solutions which *do not contain ATM* (vide infra). Atomic force microscopy (AFM) and field emission scanning electron microscopy (FE-SEM) images of the electrodes obtained after immersion in the solution of ATM indicate the formation of surfaces (average roughness 2 ± 0.1 nm) which are 3.5−4 nm high on the electrode surfaces (Figure 2A, B, C and Supporting Information, Figure S5). Note that, bare Au shows very different 2D and 3D topographic AFM images as well as FE-SEM images (Supporting Information, Figure S6 and S7). The formation of ATM modified surface is evident from the bearing ratio and roughness values obtained from the AFM analysis when compared to bare Au (Supporting Information, Figure S6 and S8). Electrochemical shielding of Au electrodes because of formation of these structures is directly indicated by large peak separations of the cathodic and anodic processes in a CV experiment of potassium ferricyanide [$K_3Fe(CN)_6$] (Supporting Information, Figure S9).[53] This behavior is similar to the electrochemical shielding observed because of the formation of self-assembled monolayer of thiols and thioethers on Au electrodes.[54] This electrochemical shielding of the Au electrodes by the ATM layer inhibits direct ORR by the Au electrode.

XPS data of Au electrode bearing layers of ATM (Figure 2D, E, and F) show the Mo $3p_{3/2}$ and $3p_{1/2}$ peaks at 395.4 and 413.2 eV; Mo $3d_{3/2}$ and Mo $3d_{5/2}$ peaks at 232.5 and 229.7 eV; N 1s peak at 400.0 eV; a major S species (I S) of S 2s, S $2p_{1/2}$, and S $2p_{3/2}$ peaks at 225.8 eV, 163.0 eV, and 161.6 eV; a minor S species (II S) of S 2s, S $2p_{1/2}$, and S $2p_{3/2}$ peaks at 226.9 eV, 164.5 eV, and 162.3 eV; O 1s peak at 532.5 eV (Supporting Information, Figure S10), respectively.[55] The characteristic peaks for Mo and N confirm the presence Mo^{VI} and NH_4^+ in the assembly.[12,37,40,56] The major S peak (both S_{2s} and S_{2p}) originates from a S^{2-} unit of a MoS_4^{2-} anion.[45] Thus the XPS data clearly indicate the presence of ATM units on the Au surface along with water. In addition to this the energies of the S_{2s} and S_{2p} ionizations of the minor S species observed originate from a S^{2-} directly bound to the Au surface. This direct interaction of S with Au is also confirmed by the slightly higher value of $4f_{7/2}$ binding energy of Au (85.0 eV) relative to bare Au (84.0 eV).[45] Therefore, these data are consistent with the formation of a multilayer of ATM attached to the Au surface via a Mo−S−Au linkage. An approximate relative atom composition of the Au bound S^{2-} and only Mo bound S^{2-} is obtained from the intensities of the S_{2p} peaks to be 1:7. Assuming that two sulfides of a MoS_4^{2-} anion bind to the Au, the above ratio would indicate that there are 14 unbound sulfides in the 4 nm high assembly, that is, 2 free sulfides from the bound MoS_4^{2-} and 12 additional sulfides from three assembled MoS_4^{2-} units. The NH_4^+ ions (the only cation present in the deposition solution) are necessary to neutralize the charge of the MoS_4^{2-} anion and provide a three-dimensional hydrogen bonding network. Similar organization (except the attachment to the Au surface) is observed in the crystal structure of ATM.[57] The height of a MoS_4^{2-} unit hydrogen bonded to the counter ammonium ion is ∼1 nm in the crystal structure. Thus, the ratio of the Au bound and only Mo bound S^{2-} (from XPS) along with the height of the multilayer (4 nm from AFM, Figure 2C) is consistent with the formation of 4 such layers. A hypothetical model of ATM assembly on Au which is consistent with the XPS data as well as the AFM data and is based on the organization of the NH_4^+ and the MoS_4^{2-} ions in ATM crystals can be proposed (a vertical cross section is represented in Figure 2G). The presence of H_2O in the material (from XPS data) may facilitate the hydrogen bonding network required to stabilize such a scaffold.

ATM modified Au electrodes are effective in producing H_2 from water *without* the presence of dissolved ATM in solution. The evolution of H_2 is confirmed via its in situ electrochemical H_2 detection using either a Pt ring (in a RRDE setup; Figure 3,

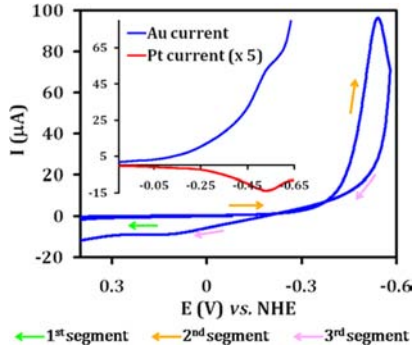

Figure 3. CV data of ATM modified Au electrode in air saturated pH 7 buffer obtained at a scan rate of 50 mV/s using Ag/AgCl as reference (data have been adjusted to potential with respect to NHE) and Pt wire as counter electrodes respectively. RRDE data is shown in the inset showing the production of H_2 by Au (blue) and its detection by Pt ring (red). The Pt ring current has been multiplied by 5 for better presentation.

inset)[23,25] or in a reverse scan in which the H_2 produced in situ is detected via its electrochemical oxidation to H^+ catalyzed by ATM (Figure 3). XPS data obtained before and after H_2 production experiment show no change in the ATM layer composition (Supporting Information, Figure S11). The plot of the i_{cat} with scan rate is linear (Supporting Information, Figure S12) indicating that the ATM adsorbed on the surface is responsible for the catalysis.[58,59] Anodic desorption experiments[60] indicate that the coverage of the ATM layers on modified electrodes is 1.34×10^{15} molecules/cm^2, 3−4 times more than the coverage of an Au surface with alkylthiol monolayers. Considering the fact that a 0.1925 cm^2 electrode bearing 1.34×10^{15} molecules/cm^2 ATM produces 0.44 ± 0.02 mL of H_2 in 10 h, the turnover number (TON) and turnover frequency (TOF) can be estimated to be $>5 \times 10^4$ and 1.4 s^{-1},

dx.doi.org/10.1021/ic402056k | *Inorg. Chem.* 2013, 52, 14168−14177

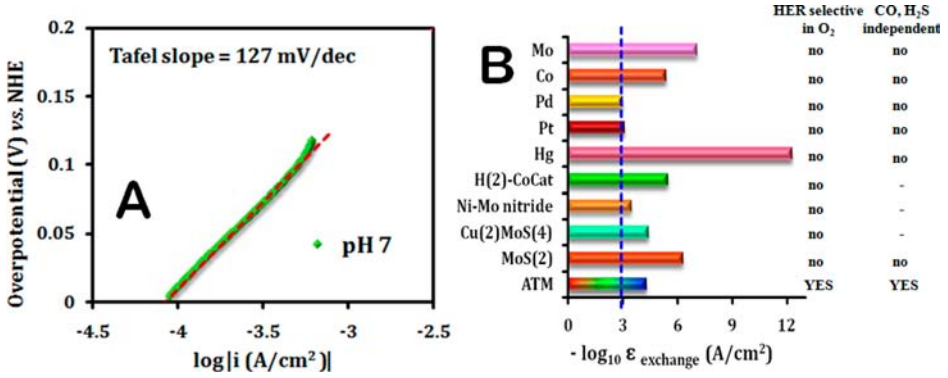

Figure 4. (**A**) Tafel plot of the corresponding CV of ATM over Au electrode obtained at 50 mV/s in pH 7 buffer is showing a Tafel slope of 127 mV/dec; (**B**) Plot of $-\log(\varepsilon_{exchange})$ (A/cm^2) of various transition and noble metals and HER catalysts versus ATM. The yellow, orange, pink, and red bars indicate that the catalysts are operative in low (acidic) pH range; green indicates neutral pH, and blue indicates high pH.

respectively. As the BE experiment was done in the presence of 1 mM ATM in solution, the TON estimated may be treated as an upper limit because the production of H_2 by solvated ATM can not be ruled out.[61] Presence of 1 mM ATM in solution does not produce significant change in the HER current when a static Au electrode is used (Supporting Information, Figure S13). Moreover these ATM modified Au electrodes show dramatic shielding of charge transfer from the electrode to dissolved species in solution as indicated by the splitting between the anodic and cathodic waves in the CV data of $K_3[Fe(CN)_6]$ (Supporting Information, Figure S9). This suggests that HER via charge transfer to the dissolved ATM species in solution is likely to be minimal.

The Tafel plot (log $|i_{cat}|$ vs overpotential) indicates that the exchange current density ($\varepsilon_{exchange}$), that is, the current density at zero overpotential for ATM modified Au electrodes (Figure 4A) is $10^{-4.25}$ at pH 7. Note that the $\varepsilon_{exchange}$ value calculated for ATM is an average of the values obtained at various scan rates (ranging from 50−2 mV/s) (Supporting Information, Figure S14). This is comparable to those obtained for noble metals like Pt ($10^{-3.1}$) and Pd ($10^{-3.0}$) in 1 N acid (Figure 4B, Supporting Information, Table S1).[62] In addition to the high $\varepsilon_{exchange}$ at neutral pH, these ATM functionalized Au electrodes are selective toward HER and do not show significant ORR under oxic conditions. The $\varepsilon_{exchange}$ of ATM on Au is comparable to those known for noble metals like Pt and Pd. Only a few HER catalysts reported earlier showed similar energy efficient H_2 generation.[12,63] Most Mo based catalyst show $\varepsilon_{exchange}$ in the order of 10^{-6} to 10^{-7}, that is, 2−3 orders of magnitute lower than ATM (Figure 4B and Supporting Information, Table S1).[8,37] The rate of HER catalysis by ATM is 1.4 s^{-1}. Given the concentration of the substrate, that is, H^+, at pH 7 is 10^{-7} M, the second order rate of HER can be as high as ~10^7 M^{-1} s^{-1}.[64] The large rate of HER is consistent with the very high current densities obtained from the Tafel plot.

The reactivity of ATM functionalized Au electrodes is very different from the reactivity of neutral MoS_x functionalized Au and GC electrodes. These electrodes, generated from anodic and cathodic deposition of MoS_x from ATM solution (Supporting Information, Figure S15), produce large H^+ reduction currents below −0.2 V under anoxic conditions in 1 N H_2SO_4 (Figure 5, blue line). These results are consistent with previous reports of Hu et al. and Jaramillo et al.[16,41] However, under oxic conditions, significant O_2 reduction currents are observed (Figure 5, red line) for modified Au

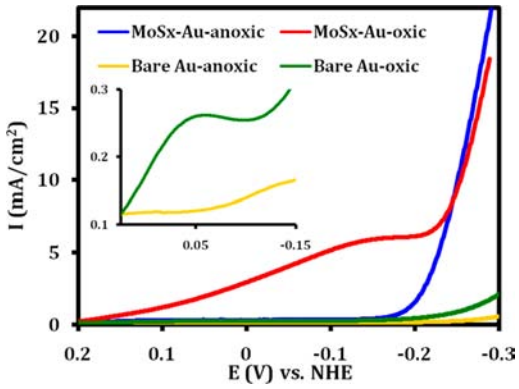

Figure 5. Linear sweep voltammetry (LSV) data of MoS_x modified Au (111) surface in 1 N H_2SO_4 solution under anoxic (blue) and oxic (red) conditions using Ag/AgCl as reference (data have been adjusted to NHE) and Pt wire as counter electrodes. Control with bare Au electrode is given in the yellow (anoxic) and green (oxic) curves.

electrodes between 0.1 and −0.2 V. The same trend is observed when a GC electrode is used, that is, HER under anoxic (Supporting Information, Figure S14, green) and ORR and HER under oxic conditions (Supporting Information, Figure S16, orange). At this point it is difficult to cogitate if this O_2 reduction activity on these electrodes is characteristic of the neutral MoS_x material or is due to exposed Au/GC electrode surfaces which can also catalyze ORR. Notably, the ORR and HER activity of the bare Au electrode under both oxic and anoxic conditions were also obtained (Figure 5), and significant oxygen reduction current could be seen along with proton reduction current.

These ATM functionalized Au surfaces can produce H_2 over a large range of pH, and a plot of the potential (E) vs pH indicates that maximum catalytic activity of H_2 generation is almost always obtained at ~20−30 mV overpotential compared to its thermodynamic potential in this entire range of pH (Figure 6). The slope of this plot is 58 mV per pH unit (Figure 6) which suggests that the H_2 generation pathway proceeds via a PCET mechanism.[10,65−67] The plot of i_{cat} vs $[H^+]$ (Supporting Information, Figure S17) indicates that the catalytic current does not vary considerably with $[H^+]$. Both the PCET behavior and the insensitivity of the catalytic current to $[H^+]$ eliminate the involvement of any metal hydride species in the catalytic cycle as H_2 evolution rate via a metal hydride species almost invariably depends on $[H^+]$.[17,23,68−70] The data

dx.doi.org/10.1021/ic402056k | Inorg. Chem. 2013, 52, 14168−14177

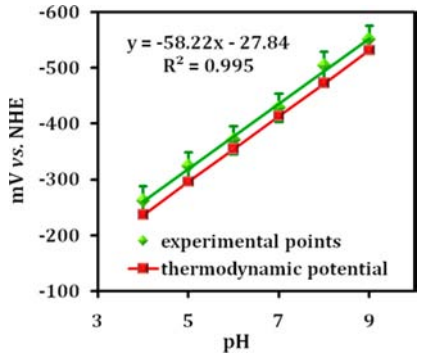

Figure 6. Plot of half peak potential, experimentally obtained from the CV data on ATM modified Au surface at various pHs at a scan rate of 50 mV/s, vs respective pHs (green) and the theoretical thermodynamic potential of H_2 production (red).

obtained at various scan rates indicate a Tafel slope of >120 mV per decade (>120 mV/dec) rise in current (Figure 4A and Supporting Information, Figure S14). A Tafel slope of >120 mV/dec is generally associated with a PCET mechanism and not a metal hydride based mechanism which generally has Tafel slope of ≤60 mV/dec.[13,63,71,72]

The electrochemical data presented here rather suits a ligand based mechanism where reduction of tetrathiomolybdate in an aqueous environment leads to the formation of $[Mo^{V}S_3SH]^{2-}$ species which then reacts with another such species in solution (in case of graphite electrode) or within the ATM multilayer (Au electrode) evolving H_2 and regenerating $[Mo^{VI}S_4]^{2-}$ (Figure 7). Ligands have been proposed to aid HER from H_2O in several molecular catalyst as well as the H_2ase enzymes itself.[12,73] In all these cases the role of the protonated ligands was to provide H^+ in the vicinity of a metal hydride species.[10,19,59,74,75] In this case the ligand may be more intimately involved in the HER reaction as indicated in the proposed mechanism (Figure 7). However additional direct experimental evidence will be necessary to establish the proposed ligand based mechanism.[76] The pH dependence of the E_{cat} reveals a PCET mechanism is at play which is known to facilitate HER catalysis. Recently, this has been demonstrated by Nocera et al. using hangman Co-porphyrin.[22] In most of the reported HER catalysts to date a metal center M^{n+} gets protonated to $[MH]^{n+1}$. This species, often proposed to have an electronic configuration of M^{n+2}-H^-, is then protonated to release H_2. This general mechanism holds for H_2ases as well.[77] In the case of ATM the protonation on reduction is likely to occur on the electron rich sulfide ligands and not on the Mo^{V} center. This is different from the pathway proposed for the molybdenum based $PY5Me_2$ Mo^{IV}=O catalysts where Mo^{II} or Mo^{I} species produced at the cathode is proposed to bind a proton and reduce it.[9] This is similar to the mechanism proposed by Artero and Tran et al. for Cu_2MoS_4.[12] However, the presence of Cu^+ in the catalyst is likely to make it vulnerable to inhibition by O_2, CO, and H_2S. The NH_4^+ group which is the counterion for the MoS_4^{2-} anion in the ATM assembly is likely to provide an efficient proton transfer pathway. These groups stay protonated at pH 7, and the proposed self-assembly of ATM where these NH_4^+ groups are in direct hydrogen bonding interaction with the catalytic MoS_4^{2-} units provides entropic advantages to the HER. In fact, when this NH_4^+ counterion is replaced with NEt_4^+ no HER activity is observed (Supporting Information, Figure S18). This clearly indicates that the NH_4^+ ions are indispensable for the HER activity of the ATM functionalized Au surfaces. This ready access to H^+, the substrate, in ATM is not present in neutral MoS_x complexes or in M_2MoS_4 (M = any monopositive metal ion) which may explain higher overpotentials required to catalyze HER in the later two cases.

To further illustrate the advantage of a ligand based H_2 evolution reaction mechanism over a metal based HER mechanism, H_2 evolution was performed in saline water (obtained from the Dead Sea) and water poisoned with S^{2-}/HS^- and CO. S^{2-}/HS^- and CO inhibits most low-valent transition metal based complexes and noble metals catalysts that catalyze HER including the naturally occurring hydrogenases. This is because S^{2-}/HS^-, being a soft ligand, and CO, being a π acid ligand, have strong affinity for low-valent metal

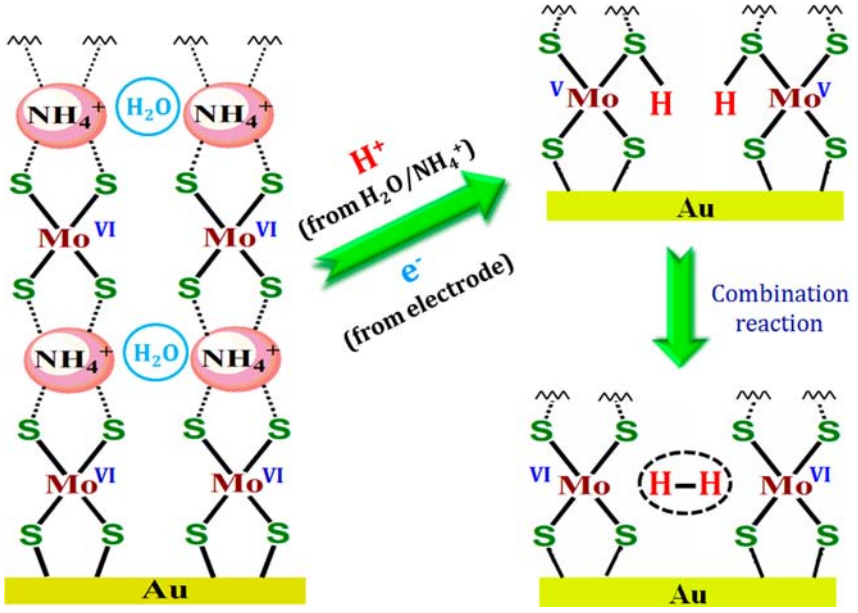

Figure 7. Proposed mechanism for H_2 evolution reaction by ATM modified Au electrodes.

dx.doi.org/10.1021/ic402056k | Inorg. Chem. 2013, 52, 14168−14177

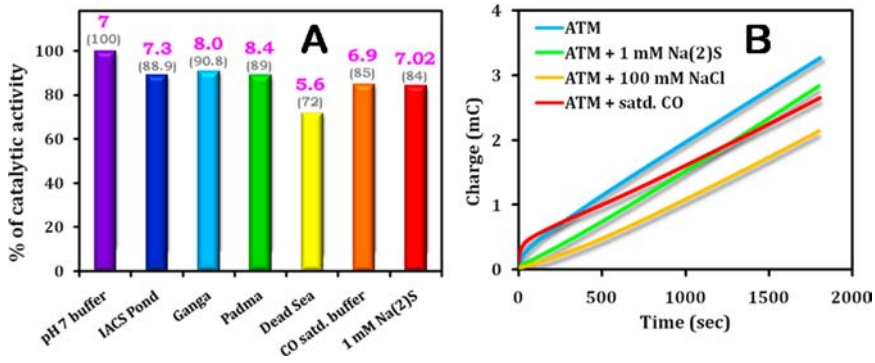

Figure 8. (**A**) Plot of percentage of catalytic activity (obtained from catalytic current) observed during H_2 production by ATM modified Au electrodes from various water sources with respect to that obtained from pH 7 buffer under oxic conditions. The values in pink represent the pHs of the different water souces and that in gray represent the percentage of original catalytic activity. (**B**) Plot of the charge consumed vs time elapsed during bulk electrolysis experiments of 1 mM ATM solution, using GCE as working electrode under anoxic conditions, in normal pH 7 buffer (blue), 1 mM Na_2S solution in pH 7 buffer (green), 100 mM NaCl solution in pH 7 buffer (yellow) and CO saturated pH 7 buffer (red), respectively. Note that the working electrode during electrolysis experiment was held at −0.55 V vs NHE.

sites which are generally the catalytically active species in HER making them veritable competitors of the substrate, H^+.[28,78] However in the case of ATM, catalytic activity was retained even in the presence of 1 mM Na_2S and saturated CO in solution (Figure 8). The lack of sensitivity to S^{2-} and CO is likely because the Mo center in ATM is high-valent which is why it does not bind CO as is the case for amorphous MoS_3.[37] Note that although the catalyst retains most of its activity in the presence of CO, it loses about 15% of its activity (Figure 8A) which is may be because of reduction of CO as suggested by Du Bois et al.[36] Retention of activity in CO saturated buffer has never been reported using a transition metal catalyst that uses a metal center to reduce H^+ including the active sites of H_2ases. The catalytic activity is retained even in a solution of 1 mM Na_2S at pH 7 for the same reasons when most conventional noble and transition metal electrode materials used for HER (e.g., Pt, Pd, Fe, Ni, Cu, Co etc.) is inhibited by H_2S. The tolerance of the ATM catalyst to these common impurities is not only limited to an Au electrode covered with ATM, HER catalyzed in homogeneous solutions of ATM using common glassy carbon electrodes is also tolerant toward these common impurities (Supporting Information, Figure S19). Thus, not surprisingly perhaps, the activity of this catalyst is retained when water from different naturally available sources is used (Figure 8A). None of these water samples were treated beyond a simple filtration process to remove insoluble particulates. Although water from these sources have variable amounts of soluble impurities (the water obtained from the delta region of the Ganges and Padma have silicates and are polluted with industrial wastes) and pHs, the tolerance of ATM functionalized Au towards a wide range of pH and toxins enables HER to remain unabated in all of these environments.

CONCLUSION

In summary, we report that ATM, a very cheap readily available laboratory chemical, can catalyze HER from water without the requirement of any additional transition metals. When an Au electrode is used, ATM assemblies are formed where the sulfide terminus of ATM binds the Au surface. Formation of such assemblies precludes a competing cathodic ORR process on the Au electrode, and this modified electrode only shows HER reactivity of ATM. The HER process catalyzed by ATM is a PCET process where the H^+ reduction is proposed to occur on the ligand. This allows retention of HER activity in water containing known inhibitors of low-valent transition and noble metals. The pH stability and resistance to inhibitors allow the ATM to function in water obtained from several natural sources. The second order rate constant of $\sim 10^7$ M^{-1} s^{-1} and low overpotential results is exchange current densities comparable to those obtained for very expensive noble metal catalysts.

EXPERIMENTAL SECTION

Materials. All reagents were of the highest grade commercially available and were used without further purification. ATM [$(NH_4)_2MoS_4$] was prepared from sodium molybdate pentahydrate [$Na_2MoO_4{\cdot}2H_2O$] and tetraethylammonium tetrathiomolybdate [$(NEt_4)_2MoS_4$] was prepared from ATM according to the reported procedures.[79] ($Na_2[MoO_4]{\cdot}5H_2O$), potassium hexafluorophosphate (KPF_6), and all buffers were purchased from Sigma-Aldrich. Disodium hydrogen phosphate dihydrate ($Na_2HPO_4{\cdot}2H_2O$), potassium chloride (KCl), conc. Hydrochloric acid (HCl), liquor NH_3 (98%), and ethanol were purchased from Merck. Sodium Sulphide nonahydrate ($Na_2S{\cdot}9H_2O$) was purchased from Rankem, India. Water used for self-assembly and all electrochemical measurements was deionized with Millipore Milli-Q purification system. Gold (Au) wafers were purchased from Platypus Technologies (1000 Å of Au on 50 Å of Ti adhesion layer on top of a Si(III) surface). Au discs for rotating ring disc electrochemistry (RRDE) experiments were purchased from Pine Instruments, U.S.A.

Synthesis of $(NH_4)_2MoS_4$ (ATM). $Na_2MoO_4{\cdot}2H_2O$ was dissolved in a 3:1 (by volume) mixture of conc. NH_4OH and H_2O. H_2S (generated by dropwise addition of 6 N HCl on pure $Na_2S{\cdot}9H_2O$) was bubbled through the ammoniacal solution until it was saturated at ambient temperature. The reaction mixture was warmed to about 60 °C for 30 min maintaining a constant pressure of H_2S. The mixture was then cooled to 4 °C and kept for 30 min. Red crystals precipitated out which were filtered and washed with cold water and ethanol. The product was finally dried under vacuum and was taken for further experiments.

Synthesis of $(NEt_4)_2MoS_4$. This complex was synthesized from 1:2 mixture of aqueous solution of ATM and tetraethylammonium bromide according to the reported procedure.[79]

Instrumentation. All electrochemical experiments were performed using a CH Instruments (model CHI710D Electrochemical Analyzer). Biopotentiostat, glassy carbon (GC), and gold (Au) working electrodes, platinum counter electrode, Ag/AgCl/satd. KCl reference electrodes, Teflon plate material evaluating cell (ALS Japan) were purchased from CH Instruments. The rotating ring disk electrochemistry (RRDE) set up from Pine Research Instrumentation (E6

dx.doi.org/10.1021/ic402056k | Inorg. Chem. 2013, 52, 14168−14177

series ChangeDisk tips with AFE6M rotor) was used to obtain the RRDE data. AFM data were recorded in a Veeco dicp II (Model no: AP-0100) instrument bearing a phosphate doped Si cantilever (1−10 ohm cm, thickness 3.5−4.5 μm, length 115−135 μm, width 30−40 μm, resonance frequency 245−287 kHz, elasticity 20−80 N/m). The surface morphology of the assembled layers were observed through a field-emission scanning electron microscope (FE-SEM, JSM-6700F), purchased from JEOL LTD, Japan. X-ray Photoelectron Spectroscopy (XPS) data were collected using an instrument from Omicron Nanotechnology GmbH, Germany (serial no. 0571).

Methods. *Construction of Electrodes: Formation of Self-Assembled Layer.* Au wafers and discs were cleaned electrochemically by sweeping several times between 1.5 V to −0.3 V in 0.5 M H_2SO_4. Depositing solutions of 1 mM concentration were prepared by simply dissolving ATM in nanopure water. Freshly cleaned Au wafers and discs were rinsed with triple distilled water, purged with N_2 gas and immersed in the solutions for self-assembly. During spectroscopic and electrochemical measurements, the electrodes were rinsed with triple distilled water followed by drying with N_2 gas.

Characterization of the Modified Surfaces. *Atomic Force Microscopy (AFM).* Freshly cut Au wafers were taken for each AFM analysis where ATM modified surfaces were made as described previously. The surfaces were thoroughly rinsed with triple distilled water before analysis. AFM data were obtained at room temperature in a Veeco dicp II instrument bearing a phosphate doped Si cantilever (1−10 ohm cm, thickness 3.5−4.5 μm, length 115−135 μm, width 30−40 μm, resonance frequency 245−287 kHz, elasticity 20−80 N/m).

Field Emission Scanning Electron Microscopy (FE-SEM). Samples were prepared in a similar way as for AFM. The surfaces were dried at room temperature and were then observed through FE-SEM applying an accelerating voltage of 5 kV after the surfaces were platinum coated. For all the FE-SEM experiments a working distance of 8 mm was used.

X-ray Photoelectron Spectroscopy (XPS). XPS was performed on the ATM modified surfaces using Mg Kα radiation (1253.6 eV) for excitation. High resolution scans, with a total energy resolution of about 1.0 eV, were recorded with pass energy of 20 eV, step size of 0.2 eV. The base pressure of the chamber initially was 1×10^{-10} mbar and during the experiment was $\sim 3 \times 10^{-10}$ mbar. Binding energy spectra were calibrated by the Ag $3d_{5/2}$ peak at 368.2 eV. An error of ±0.1 eV was estimated for all the measured values.

Electrochemical Measurements. All CV, RRDE experiment, and electrolysis experiments were done in pH 7 buffer (unless otherwise mentioned) containing 100 mM $Na_2HPO_4{\cdot}2H_2O$ and 100 mM KPF_6 (supporting electrolyte) using Pt wire as the counter electrode and Ag/AgCl as the reference electrode. All the potentials are adjusted to NHE unless otherwise stated. Note that, using GCE instead of Pt wire as a counter electrode showed no significant change in the observed results (Supporting Information, Figure S20). During experiments with natural water sources, waters were used directly after filtration without any treatments. All electrochemical experiments were performed under ambient conditions. During CV experiments on surfaces the wafers are mounted on a Teflon plate material. During RRDE experiments, an Au disc is mounted on a Pt ring assembly (Pine Instrument, AFE6RIP). Bulk electrolysis experiments with ATM modified Au discs were performed using a water jacketed electrochemical cell (Pine Instrument, RRPG138) and were rotated at an 100 rpm rate. An aqueous Ag/AgCl reference (Pine instruments, RREF0021) and Pt counter (AFCTR5) electrodes are attached to the cell through standard joints.

The active area of the Au electrode for wafers is 0.45 cm^2 and that of Au discs are 0.1925 cm^2. For GC working electrodes, the area is 0.19 cm^2.

An argon-filled glovebox was used for anaerobic solution studies with Au and GC working electrodes. The buffers were degassed accordingly by several repetitions of freeze, pump, and thaw cycles. The anaerobic studies with the RRDE setup were performed with a water jacketed cell discussed earlier where both the counter and the reference electrodes are attached to the cell with airtight joints. To make the system anaerobic, the cell was purged with Ar gas for 1 h. The reference electrode used was a commercially available aqueous Ag/AgCl electrode, and the counter electrode used was a Pt wire in all electrochemical measurements. The potentials were reported with respect to NHE by adding 200 mV to the experimentally obtained potential values. The onset potential values that are reported in Table 1 are with respect to RHE. The overpotential (η) and RHE corrected values in V were calculated using the equation given below:

$$\text{Overpotential} = (\text{applied potential}(E_{app}) - E_{pH})\ \text{V}$$

where

$$E_{pH} = (-0.059 \times \text{pH})\ \text{V}$$

$$E_{RHE} = E_{NHE} + 0.059 \times \text{pH}\ (\text{in V})$$

Detection of H_2. H_2 is generally detected by head space gas analysis by a gas chromatography (GC) fitted with appropriate detector. Such facilities are not accessible to the authors. Fontecave et al. reported an electrochemical method for detecting H_2 using RRDE.[25] In an RRDE experiment a Pt-ring encircling the working Au electrode (Figure 9) is held at a constant potential of 0.5 V. At this potential the Pt electrode oxidizes H_2, generated at the working electrode and radially diffused outward to the Pt electrode because of the hydrodynamic current produced by the rotating shaft, back to H^+ generating an oxidation current. Thus a reduction current is observed in the working electrode, and an oxidation current is observed in the Pt electrode. As a control experiment, in a standard three electrode cell, a Pt working electrode was held at a constant potential of 0.5 V and H_2 was introduced into the solution by gentle bubbling. The H_2 to H^+ current was immediately generated on the Pt electrode, and the current persisted as long as the H_2 gas was bubbled (Supporting Information, Figure S21). The current decayed as the H_2 gas bubbling was stopped. This process could be repeated several times suggesting that oxidation of H_2 back to H^+ on a Pt electrode is a reliable method for detecting formation of H_2 electrochemically in situ. Thus H_2 produced on the working electrodes was detected by oxidizing it back to H^+ on the Pt ring in a RRDE setup. Note that the Pt ring electrode held at 0.5 V can not reduce H^+ to H_2, that is, none of the H_2 produced can derive from Pt.

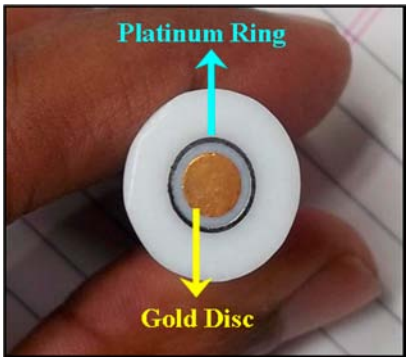

Figure 9. RRDE assembly showing the Au disc and Pt ring.

Coverage Calculation. Reductive desorption of Au surfaces fully covered (mole fraction of deposition solution =1) with ATM was done in the ethanolic solution of 0.5 mM KOH (saturated with Ar) in a Ar glovebox using Ag/AgCl and Pt-wire as the reference and the counter electrodes, respectively, and at 20 mV/s scan rate starting from −0.2 V and ending at −1.2 V. The data clearly shows a cathodic peak at −0.85 V (vs Ag/AgCl) which is for reductive desorption of ATM. The number of ATM molecules per cm^2 (Γ_i) was calculated from the area under the cathodic peak following the reported procedures.[80,81]

Determination of TON and TOF.

$$\text{TON} = \text{moles of } H_2 \text{ produced per cm}^2/\text{moles of catalyst per cm}^2$$

$$\text{TOF}(s^{-1}) = \text{TON}/\text{time of bulk electrolysis}$$

dx.doi.org/10.1021/ic402056k | Inorg. Chem. 2013, 52, 14168−14177

Bulk Electrolysis and Determination of Faradaic Yield. The bulk electrolysis experiments were performed in a water jacketed two compartment electrochemical cell and the same shaft, used for RRDE setup, fitted with ATM modified Au discs. The experiment was done in air saturated pH 7 phosphate buffer at −0.8 V vs Ag/AgCl. The rotating shaft bearing working electrode was rotated at 100 rpm speed to disperse the H_2 formed during electrolysis. The gas formed was made to flow through an outlet fitted with the cell and collected by an inverted buret setup.[23,27] Similar experiments were performed having the Pt counter electrodes in the same compartment, where the 2/3 volume of the total gas produced was taken as the amount of H_2 gas produced and was further used to calculate the FY. These experiments were repeated for 3 times, and the average FY was measured using the following equation:

$$\mathrm{FY}(\%) = [100 \times \mathrm{H_2\ produced\ (mol)} \times 2 \times 96496\ (\mathrm{C\ mol^{-1}})] / \mathrm{charge\ passed\ during\ bulk\ electrolysis\ (C)}$$

This equation gives 90% FY in neutral pH under aerobic condition for our system which means that 90% of the total electrons are used for the conversion of protons to hydrogen.

■ ASSOCIATED CONTENT

Supporting Information

AFM, FE-SEM, XPS, bulk electrolysis, LSV, and CV data. This material is available free of charge via the Internet at http://pubs.acs.org.

■ AUTHOR INFORMATION

Corresponding Author

*E-mail: icad@iacs.res.in.

Notes

The authors declare no competing financial interest.

■ ACKNOWLEDGMENTS

This research is funded by the Department of Science and Technology, India, (SR/IC/35-2009) and Department of Atomic Energy, India, (2011/36/12-BRNS). S.C., K.S., and S.D. acknowledge CSIR-SRF fellowships.

■ REFERENCES

(1) Turner, J. A. *Science* **2004**, *305*, 972.
(2) Lewis, N. S.; Nocera, D. G. *Proc. Natl. Acad. Sci.* **2006**, *103*, 15729.
(3) Krajačic, G.; Martins, R.; Busuttil, A.; Duič, N.; da Graça Carvalho, M. *Int. J. Hydrogen Energy* **2008**, *33*, 1091.
(4) Edwards, P. P.; Kuznetsov, V. L.; David, W. I. F. *Philos. Tran. R. Soc., A:* **2007**, *365*, 1043.
(5) Thoi, V. S.; Sun, Y.; Long, J. R.; Chang, C. J. *Chem. Soc. Rev.* **2013**, *42*, 2388.
(6) Artero, V.; Chavarot-Kerlidou, M.; Fontecave, M. *Angew. Chem., Int. Ed.* **2011**, *50*, 7238.
(7) Tard, C. d.; Pickett, C. J. *Chem. Rev.* **2009**, *109*, 2245.
(8) Jaramillo, T. F.; Jörgensen, K. P.; Bonde, J.; Nielsen, J. H.; Horch, S.; Chorkendorff, I. *Science* **2007**, *317*, 100.
(9) Karunadasa, H. I.; Chang, C. J.; Long, J. R. *Nature* **2010**, *464*, 1329.
(10) Karunadasa, H. I.; Montalvo, E.; Sun, Y.; Majda, M.; Long, J. R.; Chang, C. J. *Science* **2012**, *335*, 698.
(11) Merki, D.; Vrubel, H.; Rovelli, L.; Fierro, S.; Hu, X. *Chem. Sci.* **2012**, *3*, 2515.
(12) Tran, P. D.; Nguyen, M.; Pramana, S. S.; Bhattacharjee, A.; Chiam, S. Y.; Fize, J.; Field, M. J.; Artero, V.; Wong, L. H.; Loo, J.; Barber, J. *Energy Environ. Sci.* **2012**, *5*, 8912.
(13) Laursen, A. B.; Kegnaes, S.; Dahl, S.; Chorkendorff, I. *Energy Environ. Sci.* **2012**, *5*, 5577.
(14) Tang, M. L.; Grauer, D. C.; Lassalle-Kaiser, B.; Yachandra, V. K.; Amirav, L.; Long, J. R.; Yano, J.; Alivisatos, A. P. *Angew. Chem., Int. Ed.* **2011**, *50*, 10203.
(15) Tran, P. D.; Pramana, S. S.; Kale, V. S.; Nguyen, M.; Chiam, S. Y.; Batabyal, S. K.; Wong, L. H.; Barber, J.; Loo, J. *Chem.—Eur. J.* **2012**, *18*, 13994.
(16) Merki, D.; Fierro, S.; Vrubel, H.; Hu, X. *Chem. Sci.* **2011**, *2*, 1262.
(17) Stubbert, B. D.; Peters, J. C.; Gray, H. B. *J. Am. Chem. Soc.* **2011**, *133*, 18070.
(18) Sun, Y.; Bigi, J. P.; Piro, N. A.; Tang, M. L.; Long, J. R.; Chang, C. J. *J. Am. Chem. Soc.* **2011**, *133*, 9212.
(19) McNamara, W. R.; Han, Z.; Yin, C.-J.; Brennessel, W. W.; Holland, P. L.; Eisenberg, R. *Proc. Natl. Acad. Sci.* **2012**, *109*, 15594.
(20) Cobo, S.; Heidkamp, J.; Jacques, P.-A.; Fize, J.; Fourmond, V.; Guetaz, L.; Jousselme, B.; Ivanova, V.; Dau, H.; Palacin, S.; Fontecave, M.; Artero, V. *Nat. Mater.* **2012**, *11*, 802.
(21) Andreiadis, E. S.; Jacques, P.-A.; Tran, P. D.; Leyris, A.; Chavarot-Kerlidou, M.; Jousselme, B.; Matheron, M.; Pécaut, J.; Palacin, S.; Fontecave, M.; Artero, V. *Nat. Chem.* **2013**, *5*, 48.
(22) Lee, C. H.; Dogutan, D. K.; Nocera, D. G. *J. Am. Chem. Soc.* **2011**, *133*, 8775.
(23) Dey, S.; Rana, A.; Dey, S. G.; Dey, A. *ACS Catal.* **2013**, *3*, 429.
(24) Kilgore, U. J.; Roberts, J. A. S.; Pool, D. H.; Appel, A. M.; Stewart, M. P.; DuBois, M. R.; Dougherty, W. G.; Kassel, W. S.; Bullock, R. M.; DuBois, D. L. *J. Am. Chem. Soc.* **2011**, *133*, 5861.
(25) Le Goff, A.; Artero, V.; Jousselme, B.; Tran, P. D.; Guillet, N.; Métaye, R.; Fihri, A.; Palacin, S.; Fontecave, M. *Science* **2009**, *326*, 1384.
(26) Lakadamyali, F.; Kato, M.; Muresan, N. M.; Reisner, E. *Angew. Chem., Int. Ed.* **2012**, *51*, 9381.
(27) Mondal, B.; Sengupta, K.; Rana, A.; Mahammed, A.; Botoshansky, M.; Dey, S. G.; Gross, Z.; Dey, A. *Inorg. Chem.* **2013**, *52*, 3381.
(28) Vincent, K. A.; Parkin, A.; Armstrong, F. A. *Chem. Rev.* **2007**, *107*, 4366.
(29) Abou Hamdan, A.; Liebgott, P.-P.; Fourmond, V.; Gutiérrez-Sanz, O.; De Lacey, A. L.; Infossi, P.; Rousset, M.; Dementin, S. b.; Léger, C. *Proc. Natl. Acad. Sci.* **2012**, *109*, 19916.
(30) Evans, D. J.; Pickett, C. J. *Chem. Soc. Rev.* **2003**, *32*, 268.
(31) De Lacey, A. L.; Fernãndez, V. c. M.; Rousset, M.; Cammack, R. *Chem. Rev.* **2007**, *107*, 4304.
(32) Stiebritz, M. T.; Reiher, M. *Chem. Sci.* **2012**, *3*, 1739.
(33) Hinnemann, B.; Moses, P. G.; Bonde, J.; Jörgensen, K. P.; Nielsen, J. H.; Horch, S.; Chorkendorff, I.; Nørskov, J. K. *J. Am. Chem. Soc.* **2005**, *127*, 5308.
(34) Rauchfuss, T. B. *Inorg. Chem.* **2004**, *43*, 14.
(35) Rakowski DuBois, M.; DuBois, D. L. *Chem. Soc. Rev.* **2009**, *38*, 62.
(36) Appel, A. M.; DuBois, D. L.; Rakowski DuBois, M. *J. Am. Chem. Soc.* **2005**, *127*, 12717.
(37) Merki, D.; Hu, X. *Energy Environ. Sci.* **2011**, *4*, 3878.
(38) Bonde, J.; Moses, P. G.; Jaramillo, T. F.; Nørskov, J. K.; Chorkendorff, I. *Faraday Discuss.* **2009**, *140*, 219.
(39) Kim, J.; Byun, S.; Smith, A. J.; Yu, J.; Huang, J. *J. Phys. Chem. Lett.* **2013**, *4*, 1227.
(40) Vrubel, H.; Merki, D.; Hu, X. *Energy Environ. Sci.* **2012**, *5*, 6136.
(41) Vrubel, H.; Hu, X. *ACS Catal.* **2013**, *3*, 2002.
(42) Kibsgaard, J.; Chen, Z.; Reinecke, B. N.; Jaramillo, T. F. *Nat. Mater.* **2012**, *11*, 963.
(43) Li, Y.; Wang, H.; Xie, L.; Liang, Y.; Hong, G.; Dai, H. *J. Am. Chem. Soc.* **2011**, *133*, 7296.
(44) Liao, L.; Zhu, J.; Bian, X.; Zhu, L.; Scanlon, M. D.; Girault, H. H.; Liu, B. *Adv. Func. Mat.* **2013**, *23* (42), 5326−5333.
(45) Wang, T.; Liu, L.; Zhu, Z.; Papakonstantinou, P.; Hu, J.; Liu, H.; Li, M. *Energy Environ. Sci.* **2013**, *6*, 625.
(46) Chianelli, R. R.; Siadati, M. H.; De la Rosa, M. P.; Berhault, G.; Wilcoxon, J. P.; Bearden, R.; Abrams, B. L. *Catal. Rev.* **2006**, *48*, 1.

(47) Benck, J. D.; Chen, Z.; Kuritzky, L. Y.; Forman, A. J.; Jaramillo, T. F. *ACS Catal.* **2012**, *2*, 1916.
(48) McCrory, C. C. L.; Uyeda, C.; Peters, J. C. *J. Am. Chem. Soc.* **2012**, *134*, 3164.
(49) Hijazi, A.; Kemmegne-Mbouguen, J. C.; Floquet, S.; Marrot, J.; Fize, J.; Artero, V.; David, O.; Magnier, E.; Pegot, B.; Cadot, E. *Dalton Trans.* **2013**, *42*, 4848.
(50) Miah, Md. R.; Ohsaka, T. *Int. J. Electrochem. Sci.* **2012**, *7*, 697.
(51) Maruyama, J.; Inaba, M.; Ogumi, Z. *J. Electroanal. Chem.* **1998**, *458*, 175.
(52) Kongkanand, A.; Kuwabata, S. *Electrochem. Commun.* **2003**, *5*, 133.
(53) Chidsey, C. E. D. *Science* **1991**, *251*, 919.
(54) Porter, M. D.; Bright, T. B.; Allara, D. L.; Chidsey, C. E. D. *J. Am. Chem. Soc.* **1987**, *109*, 3559.
(55) Note that the peak at 532.5 eV originates from encapsulated water molecules in the assembly and not from any oxo- or oxothiomolybdates formed on the surface as can be seen clearly from the XPS data of Mo 3d region. This is also confirmed by the XPS analysis of S 2p region, i.e., region between 155 and 170 eV (Supporting Information, Figure S5B), which shows the presence of ATM over the Au surface
(56) Laurie, S. H.; Pratt, D. E.; Raynor, J. B. *Inorg. Chim. Acta* **1986**, *123*, 193.
(57) Hill, B.; Lerner, H.-W.; Bolte, M. *Acta Crystallogr., Sect. E* **2010**, *66*, i13.
(58) Thoi, V. S.; Karunadasa, H. I.; Surendranath, Y.; Long, J. R.; Chang, C. J. *Energy Environ. Sci.* **2012**, *5*, 7762.
(59) Bernhardt, P. V.; Jones, L. A. *Inorg. Chem.* **1999**, *38*, 5086.
(60) Strutwolf, J.; O'Sullivan, C. K. *Electroanalysis* **2007**, *19*, 1467.
(61) Note that when the same BE experiment was performed in the absence of ATM in solution a decay of the HER current was observed after the initial few hours which may be because of the gradual desorption of the catalyst from the electrode surface under rotating condition (required to retain a steady flux of the substrate on the electrode). However, with 1 mM ATM dissolved in the buffered solution no decay of the catalytic current or the ATM solution is observed during the electrolysis experiments lasting over 10 h. The presence of 1 mM ATM in solution during BE is thus essential to impart stability to the ATM assembly on a rotating electrode.
(62) Nørskov, J. K.; Bligaard, T.; Logadottir, A.; Kitchin, J. R.; Chen, J. G.; Pandelov, S.; Stimming, U. *J. Electrochem. Soc.* **2005**, *152*, J23.
(63) Chen, W.-F.; Sasaki, K.; Ma, C.; Frenkel, A. I.; Marinkovic, N.; Muckerman, J. T.; Zhu, Y.; Adzic, R. R. *Angew. Chem., Int. Ed.* **2012**, *51*, 6131.
(64) Assuming insignificant contribution of dissolved ATM towards the HER activity showed by ATM on Au.
(65) Hammes-Schiffer, S.; Stuchebrukhov, A. A. *Chem. Rev.* **2010**, *110*, 6939.
(66) Bard, A. J.; Faulkner, L. R. *Electrochemical Methods*; Wiley: New York, 1980.
(67) Nguyen, A. D.; Rail, M. D.; Shanmugam, M.; Fettinger, J. C.; Berben, L. A. *Inorg. Chem.* **2013**, *52* (21), 12847−12854.
(68) Roubelakis, M. M.; Bediako, D. K.; Dogutan, D. K.; Nocera, D. G. *Energy Environ. Sci.* **2012**, *5*, 7737.
(69) McNamara, W. R.; Han, Z.; Alperin, P. J.; Brennessel, W. W.; Holland, P. L.; Eisenberg, R. *J. Am. Chem. Soc.* **2011**, *133*, 15368.
(70) Hu, X.; Brunschwig, B. S.; Peters, J. C. *J. Am. Chem. Soc.* **2007**, *129*, 8988.
(71) Bonde, J.; Moses, P. G.; Jaramillo, T. F.; Nørskov, J. K.; Chorkendorff, I. *Faraday Discuss.* **2008**, *140*, 219.
(72) Conway, B. E.; Tilak, B. V. *Electrochim. Acta* **2002**, *47*, 3571.
(73) Canaguier, S.; Artero, V.; Fontecave, M. *Dalton Trans.* **2008**, 315.
(74) O'Hagan, M.; Ho, M.-H.; Yang, J. Y.; Appel, A. M.; DuBois, M. R.; Raugei, S.; Shaw, W. J.; DuBois, D. L.; Bullock, R. M. *J. Am. Chem. Soc.* **2012**, *134*, 19409.
(75) Solis, B. H.; Hammes-Schiffer, S. *J. Am. Chem. Soc.* **2012**, *134*, 15253.
(76) Attempts to obtain vibrational data on the ATM Au electrodes using SERS and ATR-FTIR were not successful.
(77) Carroll, M. E.; Barton, B. E.; Rauchfuss, T. B.; Carroll, P. J. *J. Am. Chem. Soc.* **2012**, *134*, 18843.
(78) Sethuraman, V. A.; Weidner, J. W. *Electrochim. Acta* **2010**, *55*, 5683.
(79) McDonald, J. W.; Friesen, G. D.; Rosenhein, L. D.; Newton, W. E. *Inorg. Chim. Acta* **1983**, *72*, 205.
(80) Collman, J. P.; Devaraj, N. K.; Eberspacher, T. P. A.; Chidsey, C. E. D. *Langmuir* **2006**, *22*, 2457.
(81) Sengupta, K.; Chatterjee, S.; Samanta, S.; Bandyopadhyay, S.; Dey, A. *Inorg. Chem.* **2013**, *52*, 2000.